Numerical analysis of 1.54 μm double-fused vertical-cavity lasers operating continuous-wave up to 33 °C

Joachim Piprek[a)]
University of Delaware, Materials Science Program, Newark, Delaware 19716

Dubravko I. Babic[b)] and John E. Bowers
University of California, Department of Electrical and Computer Engineering, Santa Barbara, California 93106

The first vertical-cavity surface-emitting laser diodes operating continuous-wave at room temperature at 1.54 μm emission wavelength are analyzed using a comprehensive numerical simulation procedure. These lasers employ strain-compensated InGaAsP multi-quantum wells sandwiched between GaAs/AlGaAs mirrors that are double-fused on the InP spacer layers at both sides. The model includes finite element electro-thermal simulation, transfer-matrix optical analysis, and $\mathbf{k} \cdot \mathbf{p}$ band structure calculations. Internal laser parameters are obtained by fitting experimental data at different heat sink temperatures. Intervalence band absorption is found to be the dominating loss mechanism that restricts cw operation. © *1996 American Institute of Physics.* [S0003-6951(96)03019-7]

Long-wavelength (1.3–1.6 μm) vertical-cavity surface-emitting lasers (VCSELs) are a promising new generation of light sources for long-distance optical communication systems, but continuous-wave (cw) operation of those VCSELs is restricted by internal laser heating. Recently, cw operation of 1.54 μm VCSELs up to 33 °C heat sink temperature has been achieved for the first time.[1] These lasers employ GaAs/AlGaAs distributed Bragg reflectors (DBRs) tuned to 1.55 μm that are double-fused on both sides of the InP spacer (Fig. 1). The top DBR uses 30 periods of GaAs/Al$_{0.67}$Ga$_{0.33}$As and it is covered by a metal contact on a GaAs phase matching layer to enhance reflectivity. Mirror absorption is kept low by 4×10^{17} cm^{-3} beryllium doping. DBR interfaces are parabolically graded to reduce interface electrical resistance.[2] The InGaAsP multi-quantum well (MQW) active region consists of seven quantum wells (QWs) at about 1% compressive strain and six strain-compensating barriers at about -0.9% tensile strain. The MQW is sandwiched between InP spacer layers that have been extended by thin GaAs layers on top of each fused mirror to increase the emission wavelength. The bottom 28-period GaAs/AlAs DBR is pulse doped at all interfaces, in addition to 10^{18} cm^{-3} silicon doping. Further details of the laser are given in Table I including data from Ref. 3 as well as values that have been adjusted (within reasonable limits) during the following simulation to fit experimental results. In particular, the GaAs refractive index of 3.35 is replaced by 3.38 from Ref. 4 to improve the agreement with measurements.

Numerical laser simulation is applied to analyze those VCSELs (with 12 μm top DBR diameter[1]) that exhibit the highest cw operation temperature of 33 °C. The VCSEL simulation procedure includes three main steps: (1) Two-dimensional (2D) electro-thermal finite-element analysis to obtain the internal temperature distribution $T(r,z)$ as function of the injection current I. (2) 1D calculation of the op-

tical field at the laser axis ($r=0$) using the transfer-matrix method to determine emission wavelength λ_e, threshold gain g_{th} and external quantum efficiency η_{ext} as function of I. (3) 4×4 $\mathbf{k} \cdot \mathbf{p}$ band structure and optical gain calculations for the strain-compensated MQW to finally obtain the threshold current $I_{th}(I)$. Further details of the model are described elsewhere.[5]

Experimental data obtained in pulsed laser operation are employed first to determine unknown physical parameters of the device. With the short pulse length of 100 ns and a repetition rate of 100 kHz, the active region self-heating can be neglected and the internal laser temperature is approximately that of the heat sink T_s. At $T_s = 25$ °C, the emission wavelength is 1542 nm. The optical model takes into account the temperature dependency of layer thicknesses, refractive indices, and QW absorption. The thermal red-shift of the emission wavelength is typically 0.12 nm/K and it is fitted by calibrating refractive index temperature parameters dn/dT (see Table I). The measured external quantum efficiency is 2.32% at 25 °C and it shows an Arrhenius type decrease with rising temperature.[3] This behavior can be attributed to intervalence band absorption (IVBA) within the MQW or to
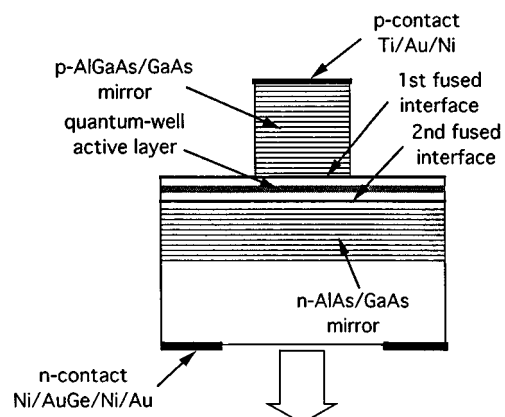

FIG. 1. Device structure of the double-fused VCSEL analyzed.

---

a)Electronic mail: piprek@udel.edu
b)Now with Hewlett-Packard, Palo Alto, CA 94304.

TABLE I. Internal parameters of the double-fused 1.54μm VCSEL at 25°C as used in the simulation (d - layer thickness, N_{dop} - doping, n - refractive index, dn/dT - temperature coefficient of n, α - absorption coefficient, κ - thermal conductivity, * indicates values that have been adjusted to fit experimental results).

Parameter	d	N_{dop}	n	dn/dT	α	κ
Unit	μm	cm^{-3}		10^{-4}K^{-1}	1/cm	W/cmK
Au/Ti (contact)	0.200	-	0.83		684000	0.67
p-GaAs	0.020	2×10^{19}	3.38*	3*	500	0.44
p-GaAs	0.182	4×10^{17}	3.38*	3*	8	0.22*
p-Al$_{0.67}$Ga$_{0.33}$As (DBR)	0.127	4×10^{17}	3.05	2	8	0.22*
p-GaAs (DBR)	0.115	4×10^{17}	3.38*	3*	8	0.44
p-GaAs (spacer)	0.020	4×10^{17}	3.38*	3*	8	0.44
p-GaAs (spacer)	0.010	4×10^{19}	3.38*	3*	1000	0.44
p-InP (spacer)	0.178*	1×10^{18}	3.17	2	24	0.68
p-InP (spacer)	0.100	1×10^{16}	3.17	2	0.24	0.68
In$_{0.76}$Ga$_{0.24}$As$_{0.82}$P$_{0.18}$ (QW)	0.0055*	-	3.5	2*	350*	0.043
In$_{0.48}$Ga$_{0.52}$As$_{0.82}$P$_{0.18}$ (barrier)	0.008	-	3.5	2*	350*	0.043
n-InP (spacer)	0.258*	5×10^{18}	3.15	2	8	0.68
n-GaAs (spacer)	0.050	1×10^{18}	3.38*	3*	6	0.44
n-GaAs (DBR)	0.115	1×10^{18}	3.38*	3*	6	0.22*
n-AlAs (DBR)	0.134	1×10^{18}	2.89	1	3	0.22*
n-GaAs (substrate)	450	5×10^{18}	3.38*	3*	5.8	0.44

carrier leakage from the MQW. Our device is designed to have high energy barriers between MQW and cladding layers (no separate confinement layers) and the leakage current is expected to be negligible.[3] Calculations confirm that carrier leakage is considerable only at high QW carrier densities that are not reached in the present case with a threshold carrier density of $N_{th} = 3.2\times10^{18}$ cm^{-3} (25 °C). IVBA at 0.8 eV photon energy is known to be strong in InGaAsP but it is expected to decrease within compressively strained QWs.[6] In our case, a large amount of holes occupies MQW states outside the quantum wells that is assumed to enhance absorption.[7] Thus, IVBA is considered within the MQW to fit the measured dependency $\eta_{ext}(T_s)$. The fit is shown in Fig. 2(a) (pulsed) and it results in an IVBA coefficient that is proportional to $\exp[-E_a/kT_s]$ with an activation energy of $E_a=0.14$ eV (k - Boltzmann constant). This temperature dependency is dominated by the number of available heavy holes at the IVBA wavevector.[8] The fitted IVBA coefficient at 25 °C is 350 cm^{-1} and it is similar to numbers measured on unstrained MQWs.[9] Further investigations of the strain-compensated MQW are required to verify this behavior. However, our high IVBA coefficient also includes temperature dependent absorption in other layers, e.g., within the DBR's or at the fused interfaces, that can hardly be separated in this analysis. Especially the p-side GaAs/InP interface is highly doped but it is close to the node of the optical field and it is therefore not expected to exhibit dominant absorption. The simulated reduction of η_{ext} with rising temperature is not only caused by absorption, but also by enhanced DBR reflectivity due to material dependent values of dn/dT.[10] The calculated threshold gain is $g_{th} = 1260$ cm^{-1} at $T_s=25$ °C and it increases with higher temperature since the MQW absorption dominates the enhanced mirror reflectivity.

The optical gain function $g(\lambda_e,N,T_a)$ is obtained from the calculated band structure of the strain-compensated MQW for any given emission wavelength λ_e, QW carrier density N, and average active region temperature T_a. In the simulation, the intended QW thickness of 6 nm had to be

reduced slightly to find agreement with measurements. The wavelength λ_g of maximum gain at 25 °C and at a typical $N = 3\times10^{18}$ cm^{-3} is 20 nm larger than the emission wavelength of 1542 nm and it exhibits a thermal red-shift of 0.9 nm/K. Thus, λ_e and λ_g are expected to coincide at $T_s \approx -1$ °C causing a minimum pulsed threshold current at
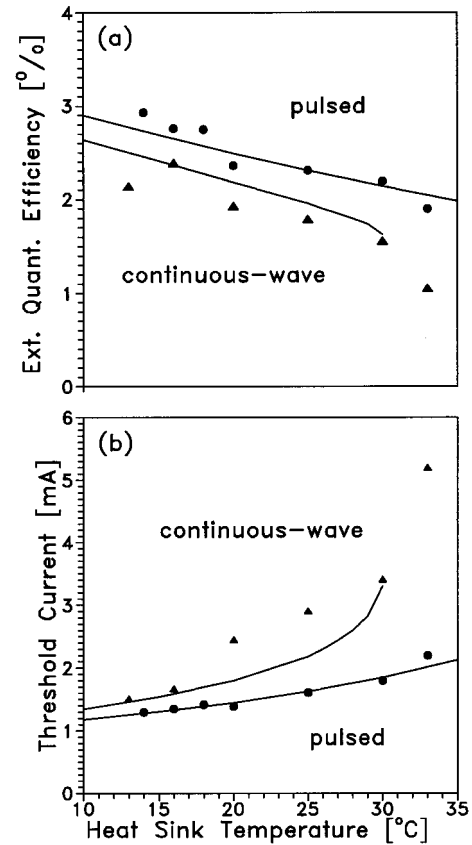

FIG. 2. (a) External quantum efficiency η_{ext} and (b) threshold current I_{th} vs heat sink temperature T_s: comparison of measurement (dots) and simulation (lines).

Appl. Phys. Lett., Vol. 68, No. 19, 6 May 1996

Piprek, Babic, and Bowers   2631

that temperature. Future device optimization is required to invert that gain offset. In our device, the lateral carrier distribution within the MQW is almost homogeneous and $g_{th}=g(\lambda_e,N_{th},T_a)$ delivers the threshold carrier density N_{th}. The measured pulse threshold currents I_{th} given in Fig. 2(b) show a typical exponential dependency on T_s with a temperature coefficient of $T_o=44$ K. The threshold current $I_{th}(T_s)$ is calculated adding up non-radiative recombination and spontaneous emission contributions within the MQW. Leakage current is neglected (see above). The rate of the spontaneous emission is obtained from the calculated band structure, its coefficient B at 25 °C is about 10^{-10} cm^3/s. The fit to the pulsed measurement [Fig. 2(b)] delivers the Shockley-Read-Hall recombination parameter $A=3.9\times10^8$ s^{-1} and the Auger coefficient $C=4.7\times10^{-29}$ cm^6/s at 25 °C. The activation energy of the Auger process is assumed to be 100 meV. All three results A, B, and C are close to recombination parameters typically measured on compressively strained quantum wells.[11] The very good agreement of both simulations with pulsed measurements (Fig. 2) confirms the physical parameters obtained. The same parameters are now employed to simulate cw operation.

CW operation causes an inhomogeneous temperature distribution $T(r,z)$ within the VCSEL due to several internal heat sources. In our simple case, the top p-DBR pillar produces most of the internal heat power due to electrical interface resistances at the metal-semiconductor contact, within the DBR, and at the fused GaAs/InP interface. At $T_s=25$ °C, a cw threshold current of $I_{th}=$ 2.91 mA and a threshold voltage of $V_{th}=$ 3.39 V are measured on our example device giving a total threshold heat power of 9.9 mW. The pillar electrical resistivity ϱ decreases with rising current density j [A/cm^2] and it is obtained from the measured cw voltage $V(I)$ reduced by the MQW Fermi voltage $V_a \approx 0.8$ V. The fit formula $\varrho(j)=0.36$ Ωcm$^2\times j^{-0.75}$ shows that the total pillar heat power rises with $I^{1.25}$ (heat power density $= \varrho j^2$). The electrical resistance of the bottom n-DBR is assumed to be small compared to that of the top pillar. The active region heat power is IV_a, its reduction by the net photon emission is neglected. In calculating the temperature distribution $T(r,z)$ as function of the injection current I, temperature dependent thermal conductivities $\kappa\propto T^{-1.375}$ are used as listed in Table I. Bulk data are applied to all layers, except the DBRs. Here, reduced values are caused by phonon mean free path restrictions in thin layers. Measurements on AlGaAs VCSELs result in thermal conductivities that are only 20% of the bulk values.[12] Due to this uncertainty, the thermal conductivity of the n-DBR is used as (only) fit-parameter to find agreement with $I_{th}(T_s)$ in cw operation, resulting in $\kappa_{DBR}=$ 0.22 W/cmK, one third of the average bulk value. The same parameter is applied to the top DBR where its impact is small in top-up mounting. The calculated temperature rise $\Delta T_a(I)$ within the active region divided by the total heat power IV gives a thermal VCSEL resistance of 1440 K/W that slightly increases with I, mainly due to the thermal lowering of $\kappa(T)$.

In order to simulate the influence of internal laser heating on optical parameters, the axial temperature profile $T(0,z)$ as function of I is utilized in the optical model. After adjusting the DBR thermal conductivity, the calculated func-tions $I_{th}(T_s)$ and $\eta_{ext}(T_s)$ in cw operation are close to the data measured (Fig. 2). Deviations might be caused by unstable heat sinking or by 2D optical effects. In the simulation, no cw lasing occurs at temperatures $T_s>30$ °C, i.e., the required threshold current $I_{th}(I)$ remains larger than the injection current. This maximum heat sink temperature of 30 °C is correlated to a maximum active region temperature of 50 °C. Both numbers are in good agreement with the experimental results of 33 °C and 55 °C measured in cw and in pulsed operation, respectively. The simulation reveals that the temperature restriction of cw operation is mainly caused by IVBA as indicated by the decrease of $\eta_{ext}(T_s)$ at higher T_s [Fig. 2(a)]. The threshold gain $g_{th}(T_s)$ builds up proportional to the IVBA leading to a nonlinear rise of $N_{th}(T_s)$ that boosts the required cw threshold current $I_{th}(T_s)$. Auger recombination exhibits the strongest increment with rising T_s but its total contribution to I_{th} remains below 50%. Further results will be published elsewhere.

In summary, the measured temperature dependencies of emission wavelength, threshold current, and external quantum efficiency in pulsed operation are utilized to obtain internal VCSEL parameters and to analyze laser operation. Intervalence band absorption seems to be the dominating loss mechanism that limits cw operation. The thermal conductivity of the fused GaAs/AlAs DBR is found to be only 33% of the value that results from bulk data. Reductions of the pillar electrical resistance as well as improvements of gain offset and heat sinking of future double-fused VCSELs are expected to allow for cw operation well above room temperature.

[1] D. I. Babic, K. Streubel, R. P. Mirin, N. M. Margalit, J. E. Bowers, E. L. Hu, D. E. Mars, L. Yang, and K. Carey, IEEE Photonics Technol. Lett. **7**, 1225 (1995).

[2] M. G. Peters, B. J. Thibeault, D. B. Young, A. C. Gossard, and L. A. Coldren, J. Vac. Sci. Technol. B **12**, 3075 (1994).

[3] D. E. Babic, Ph.D. Dissertation, University of California at Santa Barbara (1995).

[4] M. Afromowitz, Solid State Commun. **15**, 59 (1974).

[5] J. Piprek, H. Wenzel, D. Braun, H.-J. Wünsche, and F. Henneberger, SPIE Proc. **2399**, 605 (1995).

[6] P. J. A. Thijs, L. F. Tiemeijer, J. J. M. Binsma, and T. van Donger, IEEE J. Quantum Electron. **30**, 477 (1994).

[7] V. Mikhaelashvili, N. Tessler, R. Nagar, G. Eisenstein, A. G. Dentai, S. Chandrasakhar, and C. H. Joyner, IEEE Photonics Technol. Lett. **6**, 1293 (1994).

[8] Y. Suematsu and A. R. Adams, *Handbook of Semiconductor Lasers* (Chapman & Hall, New York, 1994).

[9] G. Fuchs, J. Hörer, A. Hangleiter, V. Härle, F. Scholz, R. W. Glew, and L. Goldstein, Appl. Phys. Lett. **60**, 231 (1992).

[10] J. Piprek, H. Wenzel, and G. Sztefka, IEEE Photonics Technol. Lett. **6**, 139 (1994).

[11] Y. Zou J. S. Osinski, P. Grodzinski P. D. Dapkus, W. C. Rideout, W. F. Sharfin, J. Schlafer, and F. D. Crawford, IEEE J. Quant. Electron. **29**, 1565 (1993).

[12] G. Chen, C. L. Tien, X. Wu, and J. S. Smith, J. Heat Transfer **116**, 325 (1994).